Review of Scientific Instruments

RESEARCH ARTICLE | FEBRUARY 17 2021

Ultracold neutron properties of the Eljen-299-02D deuterated scintillator

Z. Tang ; E. B. Watkins; S. M. Clayton ; S. A. Currie; D. E. Fellers; Md. T. Hassan; D. E. Hooks; T. M. Ito ; S. K. Lawrence; S. W. T. MacDonald; M. Makela; C. L. Morris ; L. P. Neukirch; A. Saunders ; C. M. O'Shaughnessy; C. Cude-Woods; J. H. Choi; A. R. Young; B. A. Zeck; F. Gonzalez; C. Y. Liu; N. C. Floyd; K. P. Hickerson; A. T. Holley; B. A. Johnson ; J. C. Lambert; R. W. Pattie

Rev. Sci. Instrum. 92, 023305 (2021)
https://doi.org/10.1063/5.0030972

Review of Scientific Instruments ARTICLE scitation.org/journal/rsi

Ultracold neutron properties of the Eljen-299-02D deuterated scintillator

Cite as: Rev. Sci. Instrum. 92, 023305 (2021); doi: 10.1063/5.0030972
Submitted: 26 September 2020 • Accepted: 19 January 2021 •
Published Online: 17 February 2021

Z. Tang,[1,a] E. B. Watkins,[1] S. M. Clayton,[1] S. A. Currie,[1] D. E. Fellers,[1] Md. T. Hassan,[1] D. E. Hooks,[1] T. M. Ito,[1] S. K. Lawrence,[1] S. W. T. MacDonald,[1] M. Makela,[1] C. L. Morris,[1] L. P. Neukirch,[1] A. Saunders,[1,b] C. M. O'Shaughnessy,[1] C. Cude-Woods,[2,c] J. H. Choi,[2] A. R. Young,[2] B. A. Zeck,[2,c] F. Gonzalez,[3] C. Y. Liu,[3] N. C. Floyd,[4,c] K. P. Hickerson,[5] A. T. Holley,[6] B. A. Johnson,[7,c] J. C. Lambert,[7,c] and R. W. Pattie[8]

AFFILIATIONS

[1]Los Alamos National Laboratory, Los Alamos, New Mexico 87545, USA
[2]North Carolina State University, Raleigh, North Carolina 27695, USA
[3]Indiana University, Bloomington, Indiana 47405, USA
[4]University of Kentucky, Lexington, Kentucky 40506, USA
[5]W. K. Kellogg Radiation Laboratory, California Institute of Technology, Pasadena, California 91125, USA
[6]Tennessee Technological University, Cookeville, Tennessee 38505, USA
[7]Utah State University, Logan, Utah 84322, USA
[8]East Tennessee State University, Johnson City, Tennessee 37614, USA

[a]**Author to whom correspondence should be addressed:** ztang@lanl.gov
[b]**Current address:** Oak Ridge National Laboratory, Oak Ridge, Tennessee 37830, USA.
[c]**Also at:** Los Alamos National Laboratory, Los Alamos, New Mexico 87545, USA.

ABSTRACT

In this paper, we report studies of the Fermi potential and loss per bounce of ultracold neutrons (UCNs) on a deuterated scintillator (Eljen-299-02D). These UCN properties of the scintillator enable its use in a wide variety of applications in fundamental neutron research.

I. INTRODUCTION

In the Standard Model of particle physics, the free neutron decay ($n \rightarrow p + e + \bar{\nu}_e$) has a characteristic lifetime τ_n of about 15 min. There are two different methods for measuring τ_n: experiments that measure the decay rate of neutrons in cold neutron beams[1–3] and experiments that measure the survival of bottled ultracold neutrons (UCNs).[4–6] By counting the number of protons emitted from neutron beta decay in a well-calibrated cold neutron beam, the beam method measures the mean time for neutrons to decay into protons, with an average result of 888.1 ± 2.0 s. In the Standard Model, this time is equivalent to the total neutron lifetime with the exception of the rare process of neutrons decaying into bound hydrogen atoms and electron antineutrinos, which has a calculated branching ratio of 4×10^{-6}.[7–9] The bottle experiments utilize trapped UCNs, which are neutrons with kinetic energy less than 350 neV. At this energy, the UCNs can undergo total external reflection on material walls, and their kinetic energy is on the same scale as their gravitational and magnetic potential energies. The UCN bottle experiments utilize these UCN properties to trap the neutrons and measure numbers that remain after a certain storage time, with an average lifetime result of 879.5 ± 0.4 s. These two methods differ by 8.7 s or 4.5 standard deviations (Fig. 1). Recently, some authors have suggested the possibility of hidden decay/oscillation channels of the neutron decay that have so far eluded detection.[10,11] Although many experiments have eliminated some of these decay channels,[12–15] some parameter space still remains.[14,16] We propose a new experiment[17] to measure the neutron beta decay lifetime by measuring the number of neutrons and the number of beta decays similar to the beam lifetime

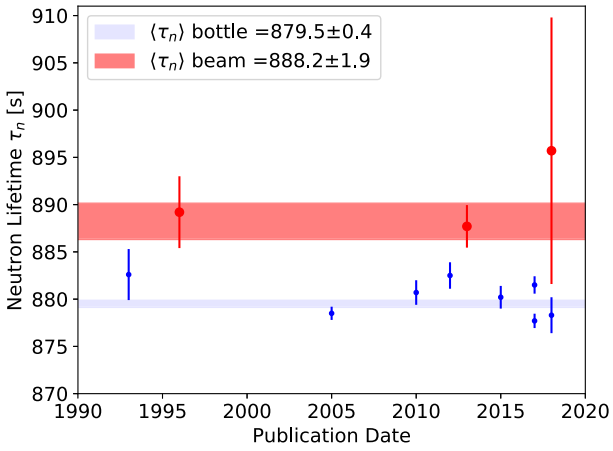

FIG. 1. Red/blue points are the data with error bars for recent beam/bottle neutron lifetime experiments. The red/blue bands are the average values for the two methods with $\pm\sigma$ error bands.

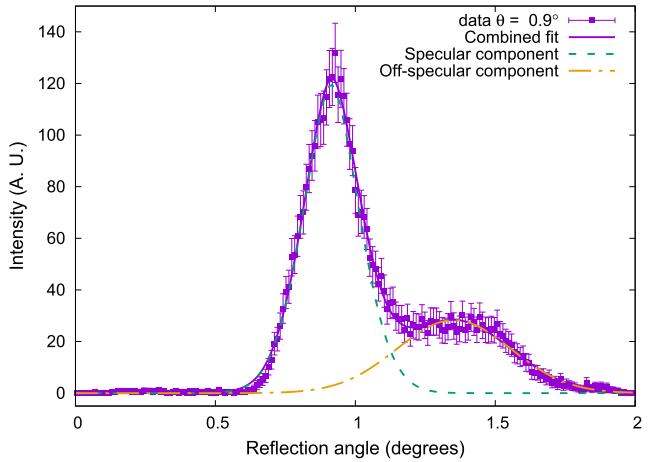

FIG. 2. Sample neutron reflectometry data for a neutron wavelength interval of 10 Å–13 Å at 0.9°. The fit is a combination of two Gaussian fits centered around the specular and off-specular component.

experiments. The main difference in the proposed experiment is that we will measure the electrons from beta decay as opposed to the protons, which will be subjected to entirely different systematic effects. The experiment will use a bottle made of deuterated polystyrene (d-PS) based scintillator to trap the UCNs and simultaneously measure the electrons from beta decay. In this paper, we report a study of the Fermi potential and loss per bounce properties of an Eljen-299-02D deuterated scintillator. Such a scintillator could also be used in other UCN related experiments due to its UCN storage properties.

II. FERMI POTENTIAL

The Fermi potential of d-PS was measured using Asterix, a time of flight neutron reflectometer at the Los Alamos Neutron Scattering Center (LANSCE).[18] Asterix views a liquid H_2 moderator providing a pulsed polychromatic cold neutron beam with wavelengths, λ, ranging from 4 Å to 13 Å. The neutron beam divergence and spot size on the sample were controlled by two sets of collimating slits. Reflectivity, R(q), is defined as the ratio of the intensity of the reflected beam to the incident beam as a function of the neutron momentum transfer vector normal to the reflecting surface, q, where $q = 4\pi \sin(\theta)/\lambda$. Total external reflection was measured up to a critical momentum transfer, $q_c = \sqrt{16\pi\beta}$, where β is the scattering length density of the sample. The relationship between β and the Fermi potential, V_F, is given in Eq. (1), where m_n is the mass of the neutron,

$$V_F = \frac{2\pi\hbar^2}{m_n}\beta. \tag{1}$$

Multiple neutron reflectometry experiments were performed to measure q_c using the polychromatic beam with incidence angles on the sample, θ, ranging from approximately 0.5°–0.9° and approximately 10% dq/q resolution. Scattered neutrons were collected using a linear ^{3}He position sensitive detector as a function of θ and λ, which simultaneously captured both the specular reflectivity signal and off-specular scattering originating from the surface roughness (Fig. 2).

The high surface roughness of the sample yielded intense off-specular scattering. The subtraction of the off-specular scattering signal from the specular reflection, R(q), was accomplished by first fitting the data to two Gaussian peaks. Only the data within the one standard deviation region of the fitted specular reflection centroid are then included in the λ to q space conversion. We suspect that the asymmetric nature of the off-specular reflection was due to geometric defects of the sample at a scale larger than the coherence length of the neutron beam. In this case, the off-specular reflections at shallow angles will be shadowed by the surface material. This background subtraction scheme of the off-specular reflection introduced a systematic uncertainty in the measurement. To mitigate the influence

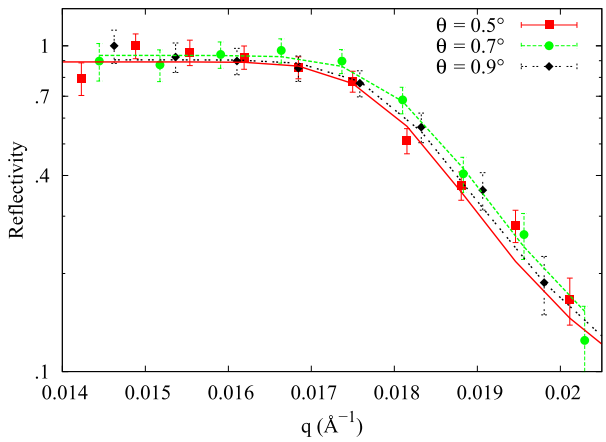

FIG. 3. Neutron reflectometry data (symbols) and fits (lines) to d-PS for three sets of incident angles. An average scattering length density, β, was obtained by fitting the Fresnel reflectivity function to the multiple datasets. Three measurements using different incident angles of the neutrons were used to ensure the accuracy of the fitted β value.

of background subtraction on the value of the Fermi potential, multiple measurements were made using different incident angles of the neutron beam on the sample (Fig. 3).

The reflectivity curves were fitted using Fresnel's law for reflection from an ideal interface, which captures the total external reflection of neutrons up to q_c followed by a q^{-4} drop in intensity. A normalization factor and the β for d-PS were the only free parameters used in the fit, and error estimates on the β parameter were based on a $\chi^2 + 1$ metric. Values obtained for β from fitting three independent measurements were $6.42 \pm 0.08 \times 10^{-6}$ Å^{-2}, $6.53 \pm 0.12 \times 10^{-6}$ Å^{-2}, and $6.48 \pm 0.11 \times 10^{-6}$ Å^{-2}, corresponding to Fermi potentials of 167.2 ± 2.1 neV, 170.0 ± 3.1 neV, and 168.7 ± 2.9 neV. Averaging the three measurements yields a β of $6.48 \pm 0.06 \times 10^{-6}$ Å^{-2}, corresponding to a Fermi potential of 168.2 ± 1.5 neV.

III. SCINTILLATOR LOSS-PER-BOUNCE MEASUREMENT

A loss-per-bounce measurement for the Eljen-299-02D scintillator was performed by measuring the lifetimes of a stainless steel UCN bottle with and without the scintillator placed inside the bottle. The volume and surface area of the bottle are 3270 cm^3 and 1350 cm^2, respectively, and the surface area of the scintillator is 292 cm^2. The UCN bottle was connected to a port off the Los Alamos UCN source[19] and was separated from the deuterium volume by a 0.001″ thick 1100 series aluminum foil. This aluminum foil has a calculated Fermi potential of 60 neV, which sets the lower bound of the UCN energy spectrum. The bottle was raised 0.635 m from the beamline to reduce the energy of the incoming UCNs, which can have energy up to the Fermi potential of the nickel–phosphorus coated source guide (213 neV).[20] This ensures that the UCN will not have enough energy to penetrate the Fermi potential of the scintillator (168 neV). The UCNs are loaded into the bottle for 300 s with the upstream gate valves open. Once the UCN density is well saturated inside the bottle, the gate valves are then closed, and the lifetime curve of the bottle is extracted by monitoring the rate of UCN loss through a 0.635 cm diameter pinhole boron film detector[21] (Fig. 4). The lifetime curves with and without the scintillator are shown in Fig. 5.

The analysis for the loss per bounce of the scintillator was performed simultaneously using the two datasets: the loss per bounce of the stainless steel UCN bottle is a fitting parameter for both datasets, and the loss per bounce of the scintillator is only relevant for the dataset with the scintillator. The spectral evolution model used to fit the two datasets is described in Eq. (2), where $N(t)$ is the number of UCN observed by the pinhole detector as a function of time, $\rho(E)$ is the initial energy spectrum of the UCN, and $\tau(E)$ is the bottle lifetime as a function of energy. An additional velocity weight accounts

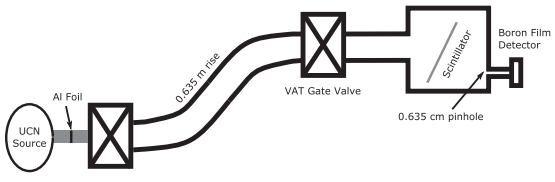

FIG. 4. Schematic diagram for the loss-per-bounce measurement.

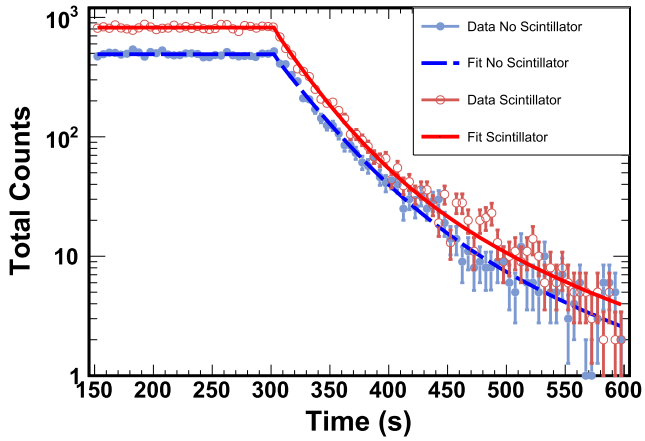

FIG. 5. Histogram of the total number counts seen by the pinhole detector for the two different run configurations as a function of time. The solid and dashed lines represent the measurements with and without the deuterated scintillator, respectively. A global fit of the two datasets was performed using two free parameters, loss per bounce of the stainless-steel bottle, and loss factor, f, of the scintillator. The equilibrium plateau of each configuration (150 s–300 s) was used to fit for the normalization factor of each dataset.

for the velocity dependence of UCN entering the pinhole detector. τ_β^{-1}, τ_{ss}^{-1}, $\tau_{pinhole}^{-1}$, and τ_{scint}^{-1} represent the UCN loss rates due to neutron lifetime, stainless steel bottle, pinhole detector, and scintillator, respectively,

$$N(t) = \int_{E_{min}}^{E_{max}} \rho(E) v e^{-t/\tau(E)} dE,$$
$$\tau(E)^{-1} = \tau_\beta^{-1} + \tau_{ss}(E)^{-1} + \tau_{pinhole}(E)^{-1} + \tau_{scint}(E)^{-1}. \quad (2)$$

In this paper, we used the initial velocity distribution as outlined in Refs. 20 and 22, where the collision rate weighted velocity distribution is $\rho v \sim v^{2.7}$. This initial spectrum is then adjusted to account for the height difference and loading time as shown in Eq. (3), where E and E_{rise} are the kinetic energies of the UCN and the rise in the height of the beamline (64.8 neV), respectively. Here, we have used an energy range of 64.8 neV–186 neV for the initial spectrum. The cut-off energy of 186 neV was used instead of the source cut-off energy of 213 neV to match the Fermi potential of the stainless steel guides downstream of the Al foil. This is a good approximation of the cut-off energy of the spectrum since the UCN bottle is filled for 300 s. The energy spectrum is then modified by $\sqrt{(E - E_{rise})/E}$ to account for the change in the UCN momentum due to the rise in the guide.[23] The Los Alamos UCN source is pulsed at 0.1 Hz. To represent the time evolution of the initial spectrum properly, we summed 31 initial spectra that have been evolved from $t = 0$ s to $t = 300$ s,

$$\rho(E, h = 0, t = 0)\ dE = E^{0.35}\ dE,$$
$$\rho(E, h = 0.635\ \text{m}, t = 0)\ dE = E^{0.35}\sqrt{\frac{E - E_{rise}}{E}}\ dE,$$
$$\rho(E, h = 0.635\ \text{m}, t = 300)\ dE = \sum_{i=0}^{30} \frac{1}{31} E^{0.35}\sqrt{\frac{E - E_{rise}}{E}} \times e^{-10i/\tau(E)}\ dE \quad (3)$$

In our model, we assume that the initial velocity directions of the UCN are sufficiently mixed that the kinetic theory for non-interacting gas applies in the calculation of the wall interaction rate [Eq. (4)], where A is the total surface area of the material, $|v|$ is the magnitude of the UCN velocity, and U is the volume of the bottle. A loss-per-bounce parameter, μ, is also added onto this equation to obtain the loss rate for each component,

$$\frac{1}{\tau_i} = \frac{A_i|v|\mu_i}{4U}. \tag{4}$$

For μ_{ss}, we assumed an energy independent loss-per-bounce parameter due to the combination of losses due to gaps in the system and the losses on the surface. For $\mu_{pinhole}$, we assumed a loss rate of unity due to the UCN detector, which is a valid assumption since the surface area for the detector is 64 times larger than the surface area of the pinhole. For μ_{scint}, an energy dependent loss-per-bounce model that integrates over all incident angles is used [Eq. (5)],[23] where V_F is the Fermi potential of the scintillator, E is the kinetic energy of the UCN, and f is the ratio of the imaginary to the real part of the Fermi potential. The fit for the loss per bounce in stainless steel and f for the scintillator is given as follows:

$$\mu_{scint}(E) = 2f\left[\frac{V_F}{E}\sin^{-1}\sqrt{\frac{E}{V_F}} - \sqrt{\frac{V_F}{E} - 1}\right]. \tag{5}$$

We have used an iterative approach in our analysis: first, initial guesses of f and μ_{ss} are used to evolve the UCN energy spectrum to 300 s; then, that energy spectrum is used as an input into a global chi-squared minimization of two datasets. The iteration is complete when the initial guess values for f and μ_{ss} match the central values from the minimization, yielding a result of $f = 4.9 \pm 0.8 \times 10^{-4}$ for the scintillator and an energy independent loss per bounce for stainless steel of $\mu_{ss} = 5.4 \pm 0.1 \times 10^{-4}$ with $\chi^2/\nu = 177.17/177$. The error in the global fit was determined by taking the limits of the $\chi^2 + 1$ region for the fit as shown in Fig. 6. We also studied the systematic effects of the input energy spectrum on the fit by varying the energy dependence of $\rho(E)$. The results showed that the input energy spectrum varied from $E^{0.6-1.0}$ for the $\chi^2 + 1$ region with a fitted f ranging from 4.86 to 4.94 $\times 10^{-4}$. Therefore, we retained the final fit parameters to f and μ_{ss} and retained $\rho(E)$ at $E^{0.85}$.

The measured μ_{ss} is larger than a previous measurement of 3.5×10^{-4},[24] but we suspect that the losses in both cases are dominated by the gaps in the joints of the vacuum assembly, and the gap area to volume ratio is smaller for long guides compared to our bottle, which accounts for the discrepancy.

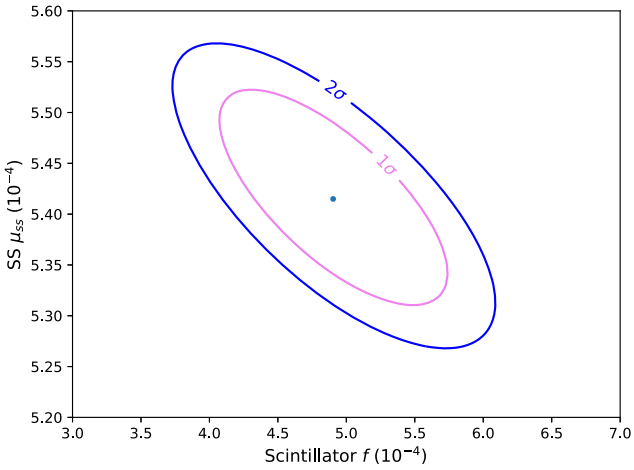

FIG. 6. Contour map showing the χ^2 minimum of the global fit as a function of f and μ_{ss}. The reduced chi-squared, χ^2/ν, is 1.0. The error (σ) in the global fit was determined using the $\chi^2 + 1$ regions.

IV. SURFACE ROUGHNESS MEASUREMENTS

The calculated value of the loss factor using the manufacturer-provided elemental and isotopic composition (97% deuterium purity) is 1×10^{-4}, which is smaller than the measured value of $4.9 \pm 0.8 \times 10^{-4}$. The hydrogen impurity in the scintillator is due to the isotopic purity of deuterated styrene monomers and the hydrogen present in the primary fluorescent emitter. One possible explanation is that the surface is rough at or below the UCN wavelength

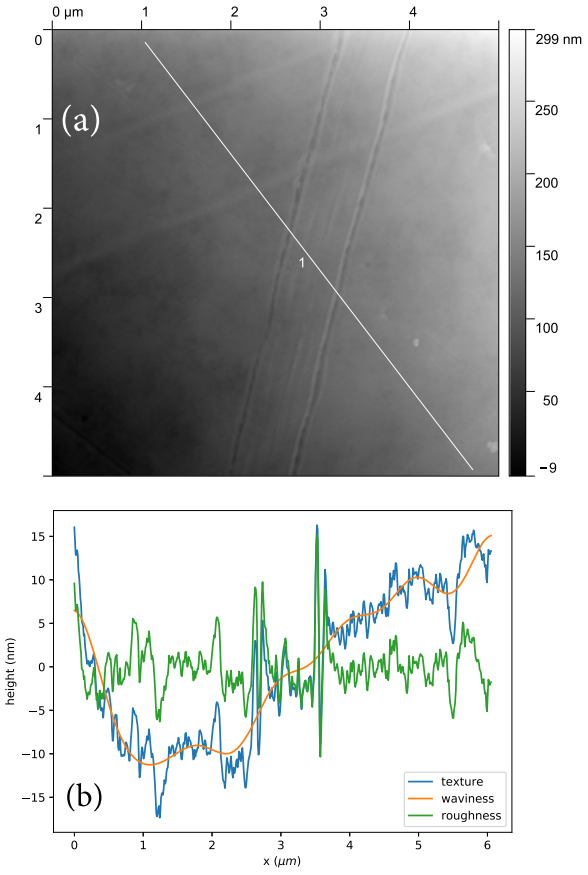

FIG. 7. (a) Sample profilometry data of a $5 \times 5\mu m^2$ spot on the deuterated polystyrene scintillator. (b) Line out from left to right as indicated by the white line in (a). The waviness was subtracted from data (texture) to obtain the roughness plot.

scale. In this case, the loss-per-bounce parameter, μ, will be modified due to the modification of the local Fermi potential.[23] Equation (6) shows the effect on the loss-per-bounce parameter, where $k_c = \sqrt{2mV_F}/\hbar$ is the critical wavelength for the neutron, σ is the rms height variation of the surface roughness, and w is the correlation length of the roughness,

$$\mu' = \mu\sqrt{1 + \frac{2\sigma^2 k_c^2}{1 + 0.85k_c w + 2k_c^2 w^2}}. \quad (6)$$

A measurement of the surface roughness of the scintillator was performed using a Bruker Dimension Icon atomic force microscope. The instrument was operated in the PeakForce tapping mode with a standard ScanAsyst-Air tip. We sampled multiple $5 \times 5\ \mu m^2$ spots on the scintillator and obtained surface roughness by fitting to line outs (Fig. 7). Since the loss-per-bounce parameter is only affected by roughness comparable to the wavelength of neutron, we estimated the surface roughness by separating out the long wavelength waviness features from the short wavelength roughness. The analysis was performed using Gwyddion, a scanning probe microscopy analysis software. We found that the average roughness ranges from 2 nm to 8 nm, and the correlation length ranges from 40 nm to 200 nm, which is only a 2% correction on the loss-per-bounce parameter in the worst case. These results indicate that the surface roughness of the scintillator is not enough to account for the differences.

V. CONCLUSION

The Fermi potential for the Eljen-299-02D scintillator was measured using a neutron reflectometry beamline at LANSCE (Asterix) with a value of 168.2 ± 1.5 neV, consistent with the calculated value of 165.8 neV. The measured loss factor of $4.9 \pm 0.8 \times 10^{-4}$ did not agree with the calculated value of 1×10^{-4}, and this result cannot be explained by the roughness of the scintillator surface. Similar anomalous UCN losses have been explained by Ref. 25, where water adsorption on the surface of the metals was the culprit. Polystyrene is hydrophobic, but one can imagine a similar adsorption mechanism with hydrocarbon molecules. To understand the origin of this anomaly, one should study the f value for the scintillator before and after baking.

Regardless of the origin of the anomalous loss, the loss factor measurement did demonstrate the utility of the scintillator in trapping UCNs and detecting electrons from neutron beta decay simultaneously, which can be used in future UCN based "beam" lifetime and beta decay correlation experiments. The measured loss factor is also sufficient to achieve the targeted statistical sensitivity for the proposed neutron beta decay lifetime experiment using a d-PS scintillator bottle. Taking the UCN spectrum and density obtained from Ref. 19, we estimate the decays per measurement cycle to be between 2180 and 5640 events for a nominal 2 l volume, with an observation time of 134 s and 206 s, respectively. The storage times for the upper- and lower-bound estimates were determined using the time when decay count is equal to the remaining UCN population. To obtain 1 s statistical sensitivity on the neutron beta decay lifetime will require approximately 180 to 460 measurement cycles.

ACKNOWLEDGMENTS

This work was supported by the Los Alamos National Laboratory LDRD Program (Project No. 20190048 ER), National Science Foundation (Grant No. PHY1914133), and U.S. Department of Energy, Office of Nuclear Physics (Grant No. DE-FG02-97ER41042). This work was performed, in part, at the Center for Integrated Nanotechnologies, an Office of Science User Facility operated for the U.S. Department of Energy (DOE) Office of Science. The authors acknowledge the support provided by the LANL Physics, AOT, MPA, and Sigma divisions. They would like to thank Eljen Technology and Charles Hurlbut for their technical support and useful discussions.

DATA AVAILABILITY

The data that support the findings of this study are available from the corresponding author upon reasonable request.

REFERENCES

[1] J. Byrne, P. G. Dawber, C. G. Habeck, S. J. Smidt, J. A. Spain, and A. P. Williams, Europhys. Lett. **33**, 187 (1996).
[2] J. S. Nico, M. S. Dewey, D. M. Gilliam, F. E. Wietfeldt, X. Fei, W. M. Snow, G. L. Greene, J. Pauwels, R. Eykens, A. Lamberty, J. V. Gestel, and R. D. Scott, Phys. Rev. C **71**, 055502 (2005).
[3] A. T. Yue, M. S. Dewey, D. M. Gilliam, G. L. Greene, A. B. Laptev, J. S. Nico, W. M. Snow, and F. E. Wietfeldt, Phys. Rev. Lett. **111**, 222501 (2013).
[4] A. P. Serebrov, V. E. Varlamov, A. G. Kharitonov, A. K. Fomin, Y. N. Pokotilovski, P. Geltenbort, I. A. Krasnoschekova, M. S. Lasakov, R. R. Taldaev, A. V. Vassiljev, and O. M. Zherebtsov, Phys. Rev. C **78**, 035505 (2008).
[5] R. W. Pattie, N. B. Callahan, C. Cude-Woods, E. R. Adamek, L. J. Broussard, S. M. Clayton, S. A. Currie, E. B. Dees, X. Ding, E. M. Engel, D. E. Fellers, W. Fox, P. Geltenbort, K. P. Hickerson, M. A. Hoffbauer, A. T. Holley, A. Komives, C.-Y. Liu, S. W. T. MacDonald, M. Makela, C. L. Morris, J. D. Ortiz, J. Ramsey, D. J. Salvat, A. Saunders, S. J. Seestrom, E. I. Sharapov, S. K. Sjue, Z. Tang, J. Vanderwerp, B. Vogelaar, P. L. Walstrom, Z. Wang, W. Wei, H. L. Weaver, J. W. Wexler, T. L. Womack, A. R. Young, and B. A. Zeck, Science **360**, 627 (2018).
[6] V. F. Ezhov, A. Z. Andreev, G. Ban, B. A. Bazarov, P. Geltenbort, A. G. Glushkov, V. A. Knyazkov, N. A. Kovrizhnykh, G. B. Krygin, O. Naviliat-Cuncic, and V. L. Ryabov, JETP Lett. **107**, 671 (2018).
[7] P. K. Kabir, Phys. Lett. B **24**, 601 (1967).
[8] L. Nemenov and A. Ovchinnikova, Sov. J. Nucl. Phys. 31(5), **659** (1980).
[9] X. Song, J. Phys. G: Nucl. Phys. **13**, 1023 (1987).
[10] Z. Berezhiani, Eur. Phys. J. C **64**, 421 (2009).
[11] B. Fornal and B. Grinstein, Phys. Rev. Lett. **120**, 191801 (2018).
[12] Z. Tang, M. Blatnik, L. J. Broussard, J. H. Choi, S. M. Clayton, C. Cude-Woods, S. Currie, D. E. Fellers, E. M. Fries, P. Geltenbort, F. Gonzalez, K. P. Hickerson, T. M. Ito, C.-Y. Liu, S. W. Macdonald, M. Makela, C. L. Morris, C. M. O'Shaughnessy, R. W. Pattie, B. Plaster, D. J. Salvat, A. Saunders, Z. Wang, A. R. Young, and B. A. Zeck, Phys. Rev. Lett. **121**, 022505 (2018).
[13] X. Sun, E. Adamek, B. Allgeier, M. Blatnik, T. J. Bowles, L. J. Broussard, M. A. Brown, R. Carr, S. Clayton, C. Cude-Woods, S. Currie, E. B. Dees, X. Ding, B. W. Filippone, A. García, P. Geltenbort, S. Hasan, K. P. Hickerson, J. Hoagland, R. Hong, G. E. Hogan, A. T. Holley, T. M. Ito, A. Knecht, C. Y. Liu, J. Liu, M. Makela, R. Mammei, J. W. Martin, D. Melconian, M. P. Mendenhall, S. D. Moore, C. L. Morris, S. Nepal, N. Nouri, R. W. Pattie, A. Pérez Galván, D. G. Phillips, R. Picker, M. L. Pitt, B. Plaster, J. C. Ramsey, R. Rios, D. J. Salvat, A. Saunders, W. Sondheim, S. Sjue, S. Slutsky, C. Swank, G. Swift, E. Tatar, R. B. Vogelaar, B. Vorndick, Z. Wang, W. Wei, J. Wexler, T. Womack, C. Wrede, A. R. Young, and B. A. Zeck, Phys. Rev. C **97**, 052501 (2018); arXiv:1803.10890.
[14] D. McKeen, A. E. Nelson, S. Reddy, and D. Zhou, Phys. Rev. Lett. **121**, 061802 (2018).

[15]Z. Berezhiani, R. Biondi, P. Geltenbort, I. A. Krasnoshchekova, V. E. Varlamov, A. V. Vassiljev, and O. M. Zherebtsov, Eur. Phys. J. C **78**, 717 (2018).
[16]J. M. Cline and J. M. Cornell, J. High Energy Phys. **2018**, 81.
[17]Z. Tang and S. M. Clayton, "Ultra-cold neutron experiment for proton branching ratio in neutron beta decay (UCNProBe)," Technical Report 20190048ER, Los Alamos National Lab LDRD Program, 2018.
[18]E. Watkins, J. Majewski, J. Baldwin, Y. Chen, N. Li, R. Hoagland, S. Yadav, X.-Y. Liu, I. Beyerlein, and N. Mara, Thin Solid Films **616**, 399 (2016).
[19]T. M. Ito, E. R. Adamek, N. B. Callahan, J. H. Choi, S. M. Clayton, C. Cude-Woods, S. Currie, X. Ding, D. E. Fellers, P. Geltenbort, S. K. Lamoreaux, C.-Y. Liu, S. MacDonald, M. Makela, C. L. Morris, R. W. Pattie, J. C. Ramsey, D. J. Salvat, A. Saunders, E. I. Sharapov, S. Sjue, A. P. Sprow, Z. Tang, H. L. Weaver, W. Wei, and A. R. Young, Phys. Rev. C **97**, 012501 (2018).
[20]R. W. Pattie, E. R. Adamek, T. Brenner, A. Brandt, L. J. Broussard, N. B. Callahan, S. M. Clayton, C. Cude-Woods, S. A. Currie, P. Geltenbort, T. M. Ito, T. Lauer, C. Y. Liu, J. Majewski, M. Makela, Y. Masuda, C. L. Morris, J. C. Ramsey, D. J. Salvat, A. Saunders, J. Schroffenegger, Z. Tang, W. Wei, Z. Wang, E. Watkins, A. R. Young, and B. A. Zeck, Nucl. Instrum. Methods Phys. Res., Sect. A **872**, 64 (2017).
[21]Z. Wang, M. Hoffbauer, C. Morris, N. Callahan, E. Adamek, J. Bacon, M. Blatnik, A. Brandt, L. Broussard, S. Clayton, C. Cude-Woods, S. Currie, E. Dees, X. Ding, J. Gao, F. Gray, K. Hickerson, A. Holley, T. Ito, C.-Y. Liu, M. Makela, J. Ramsey, R. Pattie, D. Salvat, A. Saunders, D. Schmidt, R. Schulze, S. Seestrom, E. Sharapov, A. Sprow, Z. Tang, W. Wei, J. Wexler, T. Womack, A. Young, and B. Zeck, Nucl. Instrum. Methods Phys. Res., Sect. A **798**, 30 (2015).
[22]R. Pattie, private communication (2020).
[23]R. Golub, D. Richardson, and S. K. Lamoreaux, *Ultra-Cold Neutrons* (CRC Press, 1991).
[24]A. Saunders, M. Makela, Y. Bagdasarova, H. O. Back, J. Boissevain, L. J. Broussard, T. J. Bowles, R. Carr, S. A. Currie, B. Filippone, A. García, P. Geltenbort, K. P. Hickerson, R. E. Hill, J. Hoagland, S. Hoedl, A. T. Holley, G. Hogan, T. M. Ito, S. Lamoreaux, C.-Y. Liu, J. Liu, R. R. Mammei, J. Martin, D. Melconian, M. P. Mendenhall, C. L. Morris, R. N. Mortensen, R. W. Pattie, M. Pitt, B. Plaster, J. Ramsey, R. Rios, A. Sallaska, S. J. Seestrom, E. I. Sharapov, S. Sjue, W. E. Sondheim, W. Teasdale, A. R. Young, B. Vorndick, R. B. Vogelaar, Z. Wang, and Y. Xu, Rev. Sci. Instrum. **84**, 013304 (2013).
[25]E. Korobkina, R. Golub, J. Butterworth, P. Geltenbort, and S. Arzumanov, Phys. Rev. B **70**, 035409 (2004).